RSC Advances

PAPER

View Article Online
View Journal | View Issue

Cite this: *RSC Adv.*, 2020, **10**, 34651

Influence of the rate of radiation energy on the charge-carrier kinetics application of all-inorganic $CsPbBr_3$ perovskite nanocrystals†

Virendra Kumar,[a] Vandana Nagal,[b] Rahul Kumar,[a] Shubhda Srivastava,[cd] Bipin Kumar Gupta,[d] Mahesh Kumar,[d] Aurangzeb Khurram Hafiz[b] and Kedar Singh *[a]

Received 2nd July 2020
Accepted 28th August 2020

DOI: 10.1039/d0ra05766e

rsc.li/rsc-advances

In the field of optoelectronics, all-inorganic $CsPbBr_3$ perovskite nanocrystals (PNCs) have gained significant interest on account of their superb processability and ultra-high stability among all the counterparts. In this study, we conducted an in-depth analysis of $CsPbBr_3$ PNCs using joint transient optical spectroscopies (time-resolved photoluminescence and ultrafast transient absorption) in a very comprehensive manner. In order to understand the in-depth analysis of excited-state kinetics, the transient absorption spectroscopy has been performed. The structure of interest of $CsPbBr_3$ PNCs was subjected to the rates of the radiation energy of 0.10 mW (κ_r/κ_{nr} = ~0.62) and 0.30 mW (κ_r/κ_{nr} = ~0.64). With the rate of radiation energy 0.30 mW, it was observed that there was a significant increase in hot carrier relaxation together with high radiative recombination, resulting in a decrease in charge trappings. Herein, we demonstrate that the tuning of the rate of radiation energies helps to understand the charge-carrier kinetics of $CsPbBr_3$ PNCs, which would thus improve the manufacturing of efficient photovoltaic devices.

1. Introduction

All-inorganic colloidal $CsPbX_3$ (X = Cl, Br, and I) PNCs[1] have emerged as competitive candidates in the domain of illumination, display and optoelectronics applications,[2] for instance, in solar cells,[3] light-emitting diodes,[4] photo-detectors,[5] lasers,[6] photo-catalysts,[7] luminescent solar concentrators,[8] and backlight displays.[1,9] These novel optical and electrical attributes such as the large coefficient of absorption,[10] high carrier mobility,[11] low recombination rate[1,12] together with high photoluminescence quantum yield (PLQY)[1] and superior stability[13] are the wide range attributes of $CsPbX_3$ (X = Cl, Br, and I)[1,13] in comparison to their hybrid counterparts $MAPbX_3$ (MA = CH_3NH_3, X = Cl, Br, and I).[14] From the above-mentioned features, one can easily comprehend that the kinetics of the photo-generated electron–hole[15,16] pairs inside PNCs plays a decisive role in their optoelectronic properties.[17] The time-resolved photoluminescence (TRPL)[18–29] and transient absorption (TA)[30–37] spectroscopies used to study the ultrafast photo-physical operation of charge carrier kinetics[33] in the context of the generation and recombination,[30,34] relaxation of the hot carriers,[30] properties of the interfacial charge transport[30,38–40] and pathways of negligible electron–hole confirmed with the treatment of these spectroscopic techniques, which accounts for a high PLQY[1] in the $CsPbX_3$ (X = Cl, Br, and I) PNC and its composites.

These key findings provided a broad perspective on the optimization of halide-based perovskites for optoelectronic device applications.[41,42] Substantial defect reductions and the corresponding increase in the radiative recombination rates have been reported.[43] Kamat *et al.* reported a pump fluence-dependent charge carrier kinetics study in a thin film of $CH_3NH_3PbI_3$.[44] With the variation in the halide composition from $CsPbBr_3$ to $CsPbI_3$, Kim *et al.* reported a comparative study of hot carrier cooling.[45] The pump fluence-based study of the mechanism behind hot carrier cooling in $MAPbI_3$ NCs was reported by Fu *et al.*[46] The intensity-dependent investigation of the hot carrier cooling process in $CsPbI_3$ quantum dots was examined by Feng Liu *et al.*[47] Similarly, the wavelength-dependent mechanism of the hot-carrier cooling phenomenon in $CsPbBr_3$ NC/MO_2 (M = Si, Ti, and Sn) composites was investigated by Kuang *et al.*[30] Herein, all-inclusive charge-carrier kinetics was looked into the $CsPbBr_3$ PNCs using the TRPL and the rate of radiation energy-dependent TA spectroscopy. To the best of our knowledge, we have also reported the kinetic Burstein–Moss shift attribute of the band edge

[a]*Nanotechnology Lab, School of Physical Sciences, Jawaharlal Nehru University (JNU), New Delhi-110067, India. E-mail: kedarbhu08@gmail.com; virendra2181@gmail.com*
[b]*Quantum and Nanophotonics Research Laboratory, Centre for Nanoscience and Nanotechnology, Jamia Millia Islamia (A Central University), New Delhi-110025, India*
[c]*Academy of Scientific and Innovative Research (AcSIR), Ghaziabad-201002, India*
[d]*CSIR – National Physical Laboratory, Dr. K. S. Krishnan Road, New Delhi-110012, India*

† Electronic supplementary information (ESI) available. See DOI: 10.1039/d0ra05766e

carrier aggregation in the $CsPbBr_3$ PNC material in the context of the rate of radiation dependence. As a result, the application of a 0.30 mW rate of radiation energy helps more to improve hot-carrier relaxation and significantly promotes radiative recombination in order to reduce charge trappings. In addition, the ratio obtained from the TRPL ($\kappa_r/\kappa_{nr} = \sim 0.63$) is consistent with the result obtained by TA ($\kappa_r/\kappa_{nr} = \sim 0.64$). The systematic use of different high-power laser sources for the study of charge-carrier kinetics into $CsPbBr_3$ PNCs opens up a new way of minimizing charge trapping states to make this inorganic perovskite more stable, and the observation of these findings allows for critical insights into the relatively undiscovered excited-state feature of PNCs.

2. Experimental section

2.1 Materials

Cesium carbonate (Cs_2CO_3, 99.995%), lead bromide ($PbBr_2$, 99.999%), hexane (laboratory reagent, ≥95%), oleic acid (OA, 90%), 1-octadecene (ODE, 90%) and oleylamine (OLA, 80–90%) were used in the preparation of $CsPbBr_3$ PNCs.

2.2 Formulation of cesium oleate

A cesium oleate precursor was formulated by adding 2.50 mmol of Cs_2CO_3, 8.85 mmol of oleic acid, and 158.4 mmol of 1-octadecene in a three-neck 100 mL flask, followed by vacuum desiccation for 1 h at 120 °C, and then heating the flask at 130 °C under a nitrogen atmosphere for the stark solubilization of Cs_2CO_3. The obtained solution stored in a freeze and reheated to 100 °C before using it for the preparation of all inorganic $CsPbBr_3$ PNC.

2.3 Preparation of all inorganic $CsPbBr_3$ PNC

Colloidal all-inorganic $CsPbBr_3$ PNCs were prepared using a more general modified hot-injection route. For this purpose, 1-octadecene (19.8 mmol) and lead bromide (0.188 mmol) were taken in a three-neck 25 mL flask, followed by vacuum desiccation at 120 °C for 1 h. Desiccated oleylamine (1.87 mmol) and oleic acid (1.77 mmol) were fed into the above mixture at 120 °C under a nitrogen environment. After stark solubilization of the $PbBr_2$ salt for approximately 1 h under the nitrogen environment, the temperature of the reaction was increased to 180 °C and maintained for approximately 30 min (for adjusting the size of NC); and the mixture was quenched by dipping into the ice-water bath just after the Cs-oleate (0.4 mL) solution was injected.[1]

2.4 Separation and purgation of all-inorganic $CsPbBr_3$ PNC

After cooling the mixture in an ice-water bath, the mixture was centrifuged at 10 000 rpm for 10 min in order to isolate the agglomerated PNCs. In order to prepare the long-term colloidal stable solution, we centrifuged the suspended part that has been disposed and the particles in small amounts of hexane (49.9 mmol) were re-dispersed.

2.5 Characterizations

Rigaku MiniFlex 600 with a Cu Kα radiation ($\lambda = 1.540593$ Å) source was used to obtain the powder X-ray diffraction pattern. A Cary 100 spectrometer in an absorption mode was used for the acquisition of UV-Vis spectra in the range of 400–700 nm for colloidal solutions. A Cary Eclipse (MY17060005) was used to collect the spectra in the range of 460–700 nm for the steady-state photoluminescence (PL, excitation at 450 nm). Fluorescein[1] dye was used as a reference fluorophore to calculate the photoluminescence quantum yield (PLQY). A photoluminescence lifetime spectrometer (EPL470, Edinburg Instruments Ltd with a picosecond pulsed diode laser as an exciting source having a pulse duration 93.2 ps and the peak wavelength of 466.2 nm with a maximum average power of 5 mW) was used to perform the PL lifetime measurements in a time-correlated single-photon counting mode. Transmission electron microscopy (TEM), selected area electron diffraction (SAED) and high-resolution TEM (high-angle annular dark-field scanning transmission electron microscopy JEOL 2100F) studies were carried out to understand the nanostructure in the material. An Omicron electron spectrometer of Oxford Instrument Germany equipped with a monochromatic Al Kα X-ray source ($h\nu = 1486.7$ eV) operating at 150 W was used for the elemental analysis (*i.e.*, X-ray photoelectron spectroscopy). Binding energies were in accordance with the sp^3 hybridization (C–C) carbon from OLA and OA and studied in comparison with the C1s peak (fixed at around 284.46 eV) used as a reference. An IRAffinity-1S SHIMADZU 00841 was used to record the Fourier transform-infrared spectra between 3500 cm^{-1} and 584 cm^{-1}. The TA measurements were performed using the TA spectroscopy system consisting of Ti:sapphire oscillator, regenerative amplifier coupled with an optical parametric amplifier (OPA). The oscillator is a Verdi Pumped Micra system whose output (~350 mW power with 800 nm pulses) is seeded to the regenerative amplifier, which produces 4 mJ energy output in the form of 800 nm pulses with the pulse width of 35 fs at 1 kHz repetition rate. This output was further divided into 2 portions: one is seeded into OPA (TOPAS) giving rise 290 nm to 2600 nm thus addressing from the UV to NIR region with an output pulse duration of 80 fs, while the other is introduced into spectrometer (HELIOS) moving through a delay stage of 0–8 ns, which further descends onto the sapphire crystal giving rise to a continuum of white light (420–780 nm) as a probe pulse. The former pulse of 410 nm (pump pulse) stimulates the sample under study and transfers the information of excited-state dynamics to the probe pulse. Then, the probe pulse renders the information to the detector (CMOS), and the acquired carrier dynamics have been studied using the Surface Explorer Software.

3. Results and discussion

The all-inorganic colloidal $CsPbBr_3$ PNC was prepared using a chemical route of modified hot-injection.[30] A yellowish color precipitate was obtained by centrifugation and was dispersed in hexane, a non-polar solvent.

3.1 X-ray diffraction

The powder X-ray diffraction (PXRD) pattern of the as-prepared all-inorganic colloidal $CsPbBr_3$ PNC depicted in Fig. S1† asserts an orthorhombic structure of the as-formed material, similar likewise to the earlier reports.[1]

3.2 Transmission electron microscopy (TEM)

Transmission electron microscopy (TEM) revealed that the as-synthesized $CsPbBr_3$ PNCs were of the cubic morphology and exhibited an average size of 11.58 ± 0.21 nm, as shown in Fig. 1a.[3]

3.3 Ultraviolet-visible spectroscopy and photoluminescence

Ultraviolet-visible absorption spectroscopy and photoluminescence spectroscopy were used to study the optical attributes of the all-inorganic $CsPbBr_3$ PNCs. The measured wavelength at the sharp absorption band edge was 501 nm, as displayed in Fig. 1b[30] and the emission peak was seen at 516 nm, derived from the photoluminescence (PL) emission spectrum, as depicted in Fig. 1c,[30] and PLQY was calculated to be 38.7%, as listed in Table S1.†

3.4 Time-resolved photoluminescence (TRPL) spectroscopy

The TRPL spectroscopy was further carried out in order to get further insight into the carrier kinetics in a quantitative way.[30,48–50] Using tri-exponential functions,[22] the PL fitted the decay curve pictured in Fig. 1d, and the computed values are listed in Table S2.† Although the PL spectra in Fig. 1c shows a single peak at 516 nm, the UV-Vis results in Fig. 1b indicates that the transitions of the direct bandgap of PNCs are dominated by other radiative transitions, which are further confirmed by TRPL spectroscopy as a presence of three exponential components. Moreover, the fluorescence decay lifetime (τ_1) and its contribution (β_1) corroborates with the intrinsic exciton relaxation.[50–53]

Similarly, an intermediate fluorescence decay lifetime (τ_2) and its contribution (β_2) supports interaction between excitons and phonons[50–53] and similarly ultralong-lived fluorescence decay lifetime (τ_3) and its contribution (β_3) corresponds to the interactions between excitons and defects.[52–54] The long-lived lifetime τ_3 maybe a result of less non-radiative energy transfer to the trap states.[51–54] Moreover, we have also computed the radiative (κ_r) and non-radiative (κ_{nr}) recombination decay rates,[22,55–59] as listed in Table S3.† The computed values of (κ_r) and (κ_{nr}) are 15.95 × 10^6 s^{-1} and 25.37 × 10^6 s^{-1}, respectively, and (κ_r/κ_{nr}) is about 0.63, which suggests that the non-radiative process here is relatively fast.[22,55–59]

From smaller decay lifetime component (τ_1), longer τ_{avg}, and larger (κ_r/κ_{nr}), one can infer that the as-synthesized sample features fewer trap states.[22,55,57]

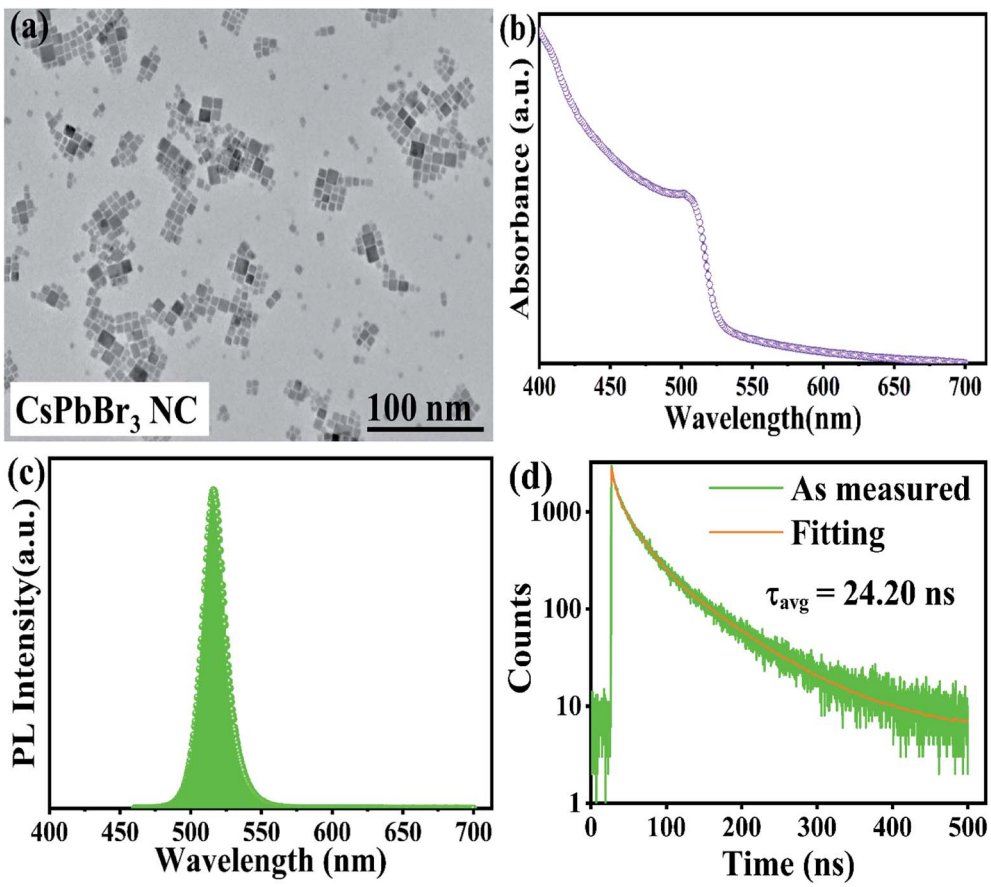

Fig. 1 (a) A TEM image; (b) ultraviolet-visible spectra; (c) PL; (d) TRPL spectra of all-inorganic $CsPbBr_3$ PNC.

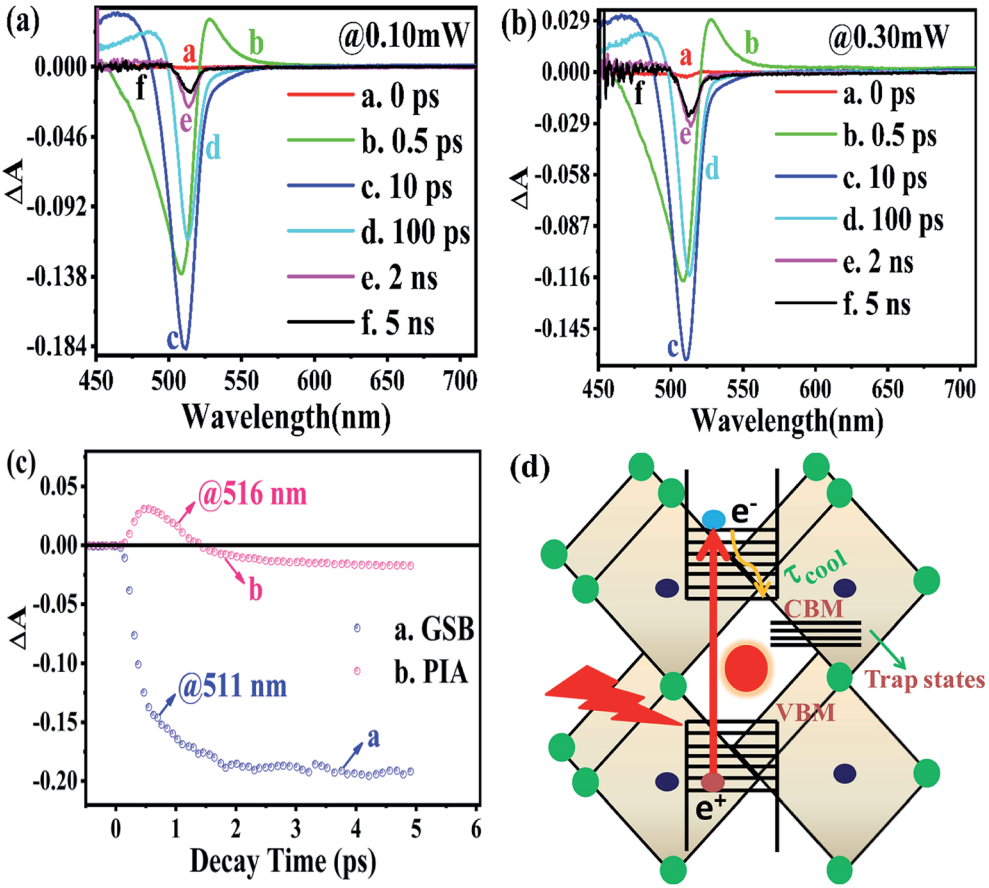

Fig. 2 Transient absorption spectroscopy under a 410 nm pump pulse of the rate of radiation energy transported by a laser source (a) at 0.10 mW; (b) at 0.30 mW; (c) the positions of PIA and GSB features explored by exploiting the transient absorption kinetics; (d) schematic depiction of the hot carrier cooling process in the $CsPbBr_3$ PNCs.

3.5 Ultrafast transient absorption spectroscopy

The TA spectroscopy was used to overcome the time resolution limitations of the TRPL technique to probe into the hot carrier kinetics.[30] The fundamental physical processes of TA have three contributions namely (i) ground state bleach (GSB), (ii) stimulated emission (SE), and (iii) photo-induced absorption (PIA). In order to produce a TA spectrum, the probe pulse is transmitted through the sample at several time delays concerning with or without the pump pulse. Therefore, a differential transmission spectrum $\Delta T(\lambda,\tau)$ ($T = (I/I_0)$, where I stands for transmitting intensity and I_0 the incident intensity of light), is produced that gives the difference of transmission measured with and without the pump pulse. If the differential transmission spectrum $\Delta T(\lambda,\tau)$ has a positive sign, then it refers to photo-induced transmission (PIT) owing to the reduced population of the ground state (*i.e.*, GSB)[37] or SE, and the negative sign stands for the photo-induced absorption (PIA)[35–37] as result of a higher population of the photo-excited states.[31,37] Similarly, if we take into consideration the differential absorption $\Delta A(\lambda,\tau)$ spectrum that quantifies the difference of absorption with and without the pump pulse. The relationship between absorption (A) and transmission (T),[60]

$$A(\lambda,\tau) = 2 - \log_{10}[T(\lambda,\tau)]$$

or

$$A(\lambda,\tau) = 2 - \log_{10}\left(\frac{I}{I_0}\right). \quad (1)$$

On adding the differential change to the above equation,[60] we get

$$A(\lambda,\tau) + \Delta A(\lambda,\tau) = 2 - \log_{10}[T(\lambda,\tau) + \Delta T(\lambda,\tau)], \quad (2)$$

or,

$$\Delta A(\lambda,\tau) = -\log_{10}\left[\frac{\Delta T(\lambda,\tau)}{T(\lambda,\tau)} + 1\right]. \quad (3)$$

From the above equations, it can be easily observed that ΔA and ΔT will have opposite signs. For example, in the case of photo-induced transmission (PIT), ΔT has a positive value, while the corresponding negative value is observed for ΔA.[60] On the other hand, for photo-induced absorption (PIA), we have a positive value for ΔA, which is a negative value for ΔT.[31,60] In this study, a pump pulse with an operating wavelength 410 nm

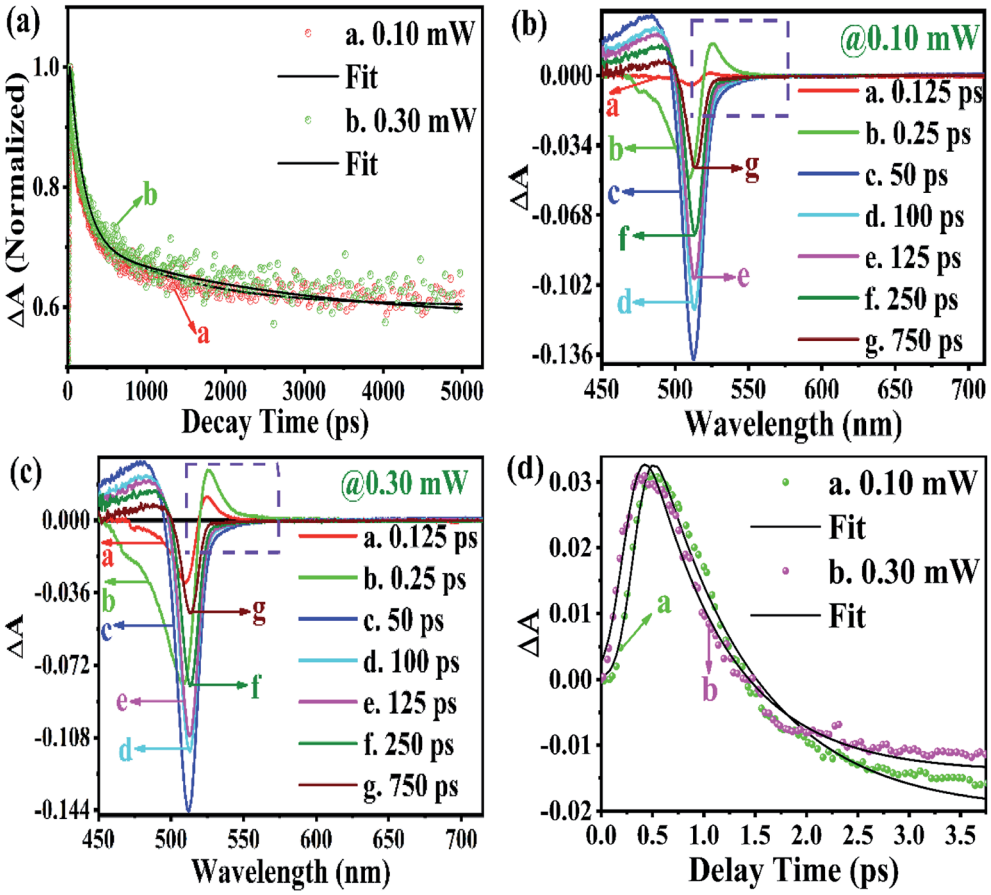

Fig. 3 (a) GSB; temporal evolutions after photo-excitation at the sort of rate of radiated energies transported by the laser source for instance (0.10 mW (b), 0.30 mW (c)) are depicted in the transient absorption (TA) spectrums of $CsPbBr_3$ PNC; (d) PIA, respectively.

was used to excite $CsPbBr_3$ PNCs, while, a white light probe was used to study the variations in induced absorption as a function of wavelength (λ) and delay time (τ). The plotted curves of TA spectra of the as-synthesized $CsPbBr_3$ PNCs for various time delays as well as at different pump powers (0.10 mW, 0.30 mW) are shown in Fig. 2. For small delay times, TA spectra with a dominant peak at 516 nm show positive PIA,[36] which steadily declines due to an increase in the delay time. The signal of GSB localized at 511 nm indicates the population occupancy of different energy states of the PNCs, as shown in Fig. 2c.[30,61–65] Fig. 2d represents the intraband state of the surface trap of PNC.[30,35,37] The ΔA intensity of the GSB signal helps to evaluate the carrier density in terms of the bandgap.[35,37,63] Fig. 3a shows that the peak intensity of GSB increases at a higher pump power of 0.30 mW as compared to that at lower power of 0.10 mW at the same delay time. As a result, the rate of recombination of charge carriers increases with increasing pump power, as shown in Fig. 3a.[30,44] The three-exponential parameters model is used to fit the decay kinetics of GSB, and the computed values are listed in Table S4.†[63]

Similarly, from the results derived from the TRPL quantitative analysis, τ_{avg} of $CsPbBr_3$ PNC for 0.10 mW is 455.37 ps, which is much lower than 884.05 ps obtained with a pump power of 0.30 mW. Similarly, as mentioned in TRPL calculations, the values of κ_r and κ_{nr} using the TA spectroscopy are $0.84 \times 10^9\ s^{-1}$ and $1.35 \times 10^9\ s^{-1}$, respectively, and κ_r/κ_{nr} is about 0.62 for $CsPbBr_3$ PNCs for the pump power of 0.10 mW.

For the pump power of 0.30 mW, κ_r and κ_{nr} are $0.44 \times 10^9\ s^{-1}$ and $0.69 \times 10^9\ s^{-1}$, respectively, and κ_r/κ_{nr} is about 0.64 (similar to the TRPL value, as listed in Table S3†), as listed in Table S5.† The values for κ_r/κ_{nr} are suggesting a fact that the non-radiative processes get suppressed in the presence of a high-power radiation source. It can be easily inferred that at a high rate of radiation energy transported (for instance 0.30 mW) to the PNCs, the values for smaller decay lifetime components, longer τ_{avg} and larger κ_r/κ_{nr}, lead to a reduction in the intermediate energy states or traps both at the surface as well as inside the PNCs resulting in the improvement of PL and PLQY of the PNCs. The PIA signal intensity is less for the lower pump power, as observed in Fig. 3b and c, and the PIA decay time was almost indistinguishable to that build-up on the GSB band-edge, as shown in Fig. 2c.[34–37,64,65] From the experimental results, we assert that when radiation energy is incident at a high rate on $CsPbBr_3$ PNCs, GSB shows a charge carrier-density involving a blue-shift of the peak wavelength together with the broadening of spectral width resulting from the aggregation of charge carriers at the band edge and can be explicated by the kinetics of Burstein–Moss shift.[35] From Fig. 3d, one can understand that the cooling time of hot carriers

is observed for $CsPbBr_3$ PNCs for the 0.10 mW pump power is 526.65 fs, while it is 417.47 fs for the pump power of 0.30 mW. Once again it can be easily understood that there is a larger decrease in the defect states as more power of radiation energy is delivered to PNCs, which can be easily observed in the improvement of PL and PLQY of the PNCs. However, such evidences were not observed during PL and TRPL measurements due to the use of the xenon lamp as a source of excitation, which was less capable of releasing the trapped energy from the defect states as observed in Fig. 3d, where we used a laser as a source of excitation with different power tuneability. Hence, the laser-induced ultrafast study is legitimate as a probe to study the kinetics of influence of the rate of radiation energy on charge carrier kinetics of $CsPbBr_3$ PNC.

4. Conclusions

In this study, we have presented the charge-carrier kinetics of all-inorganic $CsPbBr_3$ PNCs. The hot-carrier cooling physical process got augmented in the case of radiation power of 0.30 mW delivered to the $CsPbBr_3$ PNCs. The reduction in the charge trapping states by a factor of 1.03 was observed compared to the radiation power of 0.10 mW incident on the $CsPbBr_3$ PNCs, which was analysed by the ultrafast transient absorption spectroscopy. In our work, we observe that with higher radiation energy (0.30 mW) in the context of transient absorption spectroscopy, it is easier to suppress the intermediate energy states or charge trapping states, resulting in the enhancement of PL and PLQY of the PNCs. The current findings make perovskite NCs highly promising and more competitive applicant for future device applications.

Conflicts of interest

There are no conflicts to declare.

Acknowledgements

This work supported financially by the UGC-JRF as well as AIRF JNU for allowing all the required characterization facilities. A grant furnished by the SERB-DST project (EEQ/2016/000652), funded by Govt. of India, as well appreciatively acknowledged.

References

1 L. Protesescu, S. Yakunin, M. I. Bodnarchuk, F. Krieg, R. Caputo, C. H. Hendon, R. X. Yang, A. Walsh and M. V. Kovalenko, *Nano Lett.*, 2015, **15**, 3692–3696.
2 Y. Chang, Y. J. Yoon, G. Li, E. Xu, S. Yu, C.-H. Lu, Z. Wang, Y. He, C. H. Lin and B. K. Wagner, *ACS Appl. Mater. Interfaces*, 2018, **10**, 37267–37276.
3 H. Liu, Z. Liu, W. Xu, L. Yang, Y. Liu, D. Yao, D. Zhang, H. Zhang and B. Yang, *ACS Appl. Mater. Interfaces*, 2019, **11**, 14256–14265.
4 B. Xin, Y. Pak, S. Mitra, D. Almalawi, N. Alwadai, Y. Zhang and I. S. Roqan, *ACS Appl. Mater. Interfaces*, 2019, **11**, 5223–5231.
5 N. J. Jeon, J. H. Noh, W. S. Yang, Y. C. Kim, S. Ryu, J. Seo and S. I. Seok, *Nature*, 2015, **517**, 476–480.
6 W. S. Yang, J. H. Noh, N. J. Jeon, Y. C. Kim, S. Ryu, J. Seo and S. I. Seok, *Science*, 2015, **348**, 1234–1237.
7 H. Cho, S.-H. Jeong, M.-H. Park, Y.-H. Kim, C. Wolf, C.-L. Lee and J. H. Heo, *Science*, 2015, **350**, 1222–1225.
8 N. Wang, L. Cheng, R. Ge, S. Zhang, Y. Miao, W. Zou, C. Yi, Y. Sun, Y. Cao and R. Yang, *Nat. Photonics*, 2016, **10**, 699–704.
9 B. R. Sutherland and E. H. Sargent, *Nat. Photonics*, 2016, **10**, 295–302.
10 S. Chen, C. Teng, M. Zhang, Y. Li, D. Xie and G. Shi, *Adv. Mater.*, 2016, **28**, 5969–5974.
11 D. Li, D. Zhou, W. Xu, X. Chen, G. Pan, X. Zhou, N. Ding and H. Song, *Adv. Funct. Mater.*, 2018, **28**, 1804429.
12 J. Luo, S. Li, H. Wu, Y. Zhou, Y. Li, J. Liu, J. Li, K. Li, F. Yi and G. Niu, *ACS Photonics*, 2017, **5**, 398–405.
13 X. Wu, B. Zhou, J. Zhou, Y. Chen, Y. Chu and J. Huang, *Small*, 2018, **14**, 1800527.
14 J. Yang, K. Liu, Z. Cheng, P. Jing, Q. Ai, X. Chen, B. Li, Z. Zhang, L. Zhang and H. Zhao, *ACS Appl. Mater. Interfaces*, 2018, **10**, 34744–34750.
15 S. W. Eaton, M. Lai, N. A. Gibson, A. B. Wong, L. Dou, J. Ma, L.-W. Wang, S. R. Leone and P. Yang, *Proc. Natl. Acad. Sci. U. S. A.*, 2016, **113**, 1993–1998.
16 Y. Wang, X. Li, J. Song, L. Xiao, H. Zeng and H. Sun, *Adv. Mater.*, 2015, **27**, 7101–7108.
17 C. H. Lin, Q. Zeng, E. Lafalce, M. J. Smith, S. T. Malak, J. Jung, Y. J. Yoon, Z. Lin, Z. V. Vardeny and V. V. Tsukruk, *Adv. Opt. Mater.*, 2017, **5**, 1700011.
18 C. H. Lin, Q. Zeng, E. Lafalce, S. Yu, M. J. Smith, Y. J. Yoon, Y. Chang, Y. Jiang, Z. Lin and Z. V. Vardeny, *Adv. Opt. Mater.*, 2018, **6**, 1800474.
19 Y.-F. Xu, M.-Z. Yang, B.-X. Chen, X.-D. Wang, H.-Y. Chen, D.-B. Kuang and C.-Y. Su, *J. Am. Chem. Soc.*, 2017, **139**, 5660–5663.
20 J. Hou, S. Cao, Y. Wu, Z. Gao, F. Liang, Y. Sun, Z. Lin and L. Sun, *Chem.–Eur. J.*, 2017, **23**, 9481–9485.
21 F. Meinardi, Q. A. Akkerman, F. Bruni, S. Park, M. Mauri, Z. Dang, L. Manna and S. Brovelli, *ACS Energy Lett.*, 2017, **2**, 2368–2377.
22 J. Tong, J. Wu, W. Shen, Y. Zhang, Y. Liu, T. Zhang, S. Nie and Z. Deng, *ACS Appl. Mater. Interfaces*, 2019, **11**, 9317–9325.
23 J. Song, J. Li, X. Li, L. Xu, Y. Dong and H. Zeng, *Adv. Mater.*, 2015, **27**, 7162–7167.
24 A. Swarnkar, A. R. Marshall, E. M. Sanehira, B. D. Chernomordik, D. T. Moore, J. A. Christians, T. Chakrabarti and J. M. Luther, *Science*, 2016, **354**, 92–95.
25 P. Ramasamy, D.-H. Lim, B. Kim, S.-H. Lee, M.-S. Lee and J.-S. Lee, *Chem. Commun.*, 2016, **52**, 2067–2070.
26 L. Protesescu, S. Yakunin, S. Kumar, J. Bär, F. Bertolotti, N. Masciocchi, A. Guagliardi, M. Grotevent, I. Shorubalko and M. I. Bodnarchuk, *ACS Nano*, 2017, **11**, 3119–3134.
27 M. A. Prelas, C. L. Weaver, M. L. Watermann, E. D. Lukosi, R. J. Schott and D. A. Wisniewski, *Prog. Nucl. Energy*, 2014, **75**, 117–148.

28 M. Sychov, A. Kavetsky, G. Yakubova, G. Walter, S. Yousaf, Q. Lin, D. Chan, H. Socarras and K. Bower, *Appl. Radiat. Isot.*, 2008, **66**, 173–177.
29 S. Kumar, 2015, arXiv preprint arXiv:1511.07427.
30 J.-F. Liao, Y.-F. Xu, X.-D. Wang, H.-Y. Chen and D.-B. Kuang, *ACS Appl. Mater. Interfaces*, 2018, **10**, 42301–42309.
31 R. Berera, R. van Grondelle and J. T. Kennis, *Photosynth. Res.*, 2009, **101**, 105–118.
32 Y. Yamada, T. Nakamura, M. Endo, A. Wakamiya and Y. Kanemitsu, *J. Am. Chem. Soc.*, 2014, **136**, 11610–11613.
33 M. T. Trinh, X. Wu, D. Niesner and X.-Y. Zhu, *J. Mater. Chem. A*, 2015, **3**, 9285–9290.
34 N. S. Makarov, S. Guo, O. Isaienko, W. Liu, I. Robel and V. I. Klimov, *Nano Lett.*, 2016, **16**, 2349–2362.
35 M. B. Price, J. Butkus, T. C. Jellicoe, A. Sadhanala, A. Briane, J. E. Halpert, K. Broch, J. M. Hodgkiss, R. H. Friend and F. Deschler, *Nat. Commun.*, 2015, **6**, 8420.
36 Y. Zhai, C. X. Sheng, C. Zhang and Z. V. Vardeny, *Adv. Funct. Mater.*, 2016, **26**, 1617–1627.
37 Y. Yang, D. P. Ostrowski, R. M. France, K. Zhu, J. Van De Lagemaat, J. M. Luther and M. C. Beard, *Nat. Photonics*, 2016, **10**, 53–59.
38 Y. Fang, C. Bi, D. Wang and J. Huang, *ACS Energy Lett.*, 2017, **2**, 782–794.
39 H. S. Rao, W. G. Li, B. X. Chen, D. B. Kuang and C. Y. Su, *Adv. Mater.*, 2017, **29**, 1602639.
40 M. He, F. Qiu and Z. Lin, *J. Phys. Chem. Lett.*, 2013, **4**, 1788–1796.
41 K. Wu, G. Liang, Q. Shang, Y. Ren, D. Kong and T. Lian, *J. Am. Chem. Soc.*, 2015, **137**, 12792–12795.
42 J.-S. Yao, J. Ge, B.-N. Han, K.-H. Wang, H.-B. Yao, H.-L. Yu, J.-H. Li, B.-S. Zhu, J.-Z. Song and C. Chen, *J. Am. Chem. Soc.*, 2018, **140**, 3626–3634.
43 M. Zhang, H. Yu, M. Lyu, Q. Wang, J.-H. Yun and L. Wang, *Chem. Commun.*, 2014, **50**, 11727–11730.
44 J. S. Manser and P. V. Kamat, *Nat. Photonics*, 2014, **8**, 737–743.
45 H. Chung, S. I. Jung, H. J. Kim, W. Cha, E. Sim, D. Kim, W.-K. Koh and J. Kim, *Angew. Chem.*, 2017, **56**, 4160–4164.
46 J. Fu, Q. Xu, G. Han, B. Wu, C. H. A. Huan, M. L. Leek and T. C. Sum, *Nat. Commun.*, 2017, **8**, 1–9.
47 F. Liu, Y. Zhang, C. Ding, S. Kobayashi, T. Izuishi, N. Nakazawa, T. Toyoda, T. Ohta, S. Hayase and T. Minemoto, *ACS Nano*, 2017, **11**, 10373–10383.
48 F. Zhang, H. Zhong, C. Chen, X.-g. Wu, X. Hu, H. Huang, J. Han, B. Zou and Y. Dong, *ACS Nano*, 2015, **9**, 4533–4542.
49 X. Li, Y. Wu, S. Zhang, B. Cai, Y. Gu, J. Song and H. Zeng, *Adv. Funct. Mater.*, 2016, **26**, 2435–2445.
50 Z. Hu, Z. Liu, Y. Bian, S. Li, X. Tang, J. Du, Z. Zang, *et al.*, *Adv. Opt. Mater.*, 2018, **6**, 1700997.
51 S. Sun, D. Yuan, Y. Xu, A. Wang and Z. Deng, *ACS Nano*, 2016, **10**, 3648–3657.
52 C. Bi, S. Wang, Wen Wen, J. Yuan, G. Cao and J. Tian, *J. Phys. Chem. C*, 2018, **122**, 5151–5160.
53 Z. Liang, S. Zhao, Z. Xu, B. Qiao, P. Song, D. Gao and X. Xu, *ACS Appl. Mater. Interfaces*, 2016, **8**, 28824–28830.
54 H. Shi, X. Zhang, X. Sun, R. Chen and X. Zhang, *J. Phys. Chem. C*, 2019, **123**, 19844–19850.
55 G. Li, J. Huang, H. Zhu, Y. Li, J.-X. Tang and Y. Jiang, *Chem. Mater.*, 2018, **30**, 6099–6107.
56 Z. Liu, Y. Zhang, Y. Fan, Z. Chen, Z. Tang, J. Zhao, Y. Lv, *et al.*, *ACS Appl. Mater. Interfaces*, 2018, **10**, 13053–13061.
57 N. Kawano, M. Koshimizu, Y. Sun, N. Yahaba, Y. Fujimoto, T. Yanagida and K. Asai, *J. Phys. Chem. C*, 2014, **118**, 9101–9106.
58 Z. Yuan, S. Yu, Y. Tian, Y. Xin and B. Ma, *Chem. Commun.*, 2015, **51**, 16385–16388.
59 Z. Shi, S. Li, Y. Li, H. Ji, X. Li, D. Wu, T. Xu, *et al.*, *ACS Nano*, 2018, **12**, 1462–1472.
60 K. E. Knowles, M. D. Koch and J. L. Shelton, *J. Mater. Chem. C*, 2018, **6**, 11853–11867.
61 P. Maity, J. Dana and H. N. Ghosh, *J. Phys. Chem. C*, 2016, **120**, 18348–18354.
62 S. Sarkar, V. K. Ravi, S. Banerjee, G. R. Yettapu, G. B. Markad, A. Nag and P. Mandal, *Nano Lett.*, 2017, **17**, 5402–5407.
63 X. Luo, G. Liang, Y. Han, Y. Li, T. Ding, S. He, X. Liu and K. Wu, *J. Am. Chem. Soc.*, 2020, **142**, 11270–11278.
64 J. Aneesh, A. Swarnkar, V. K. Ravi, R. Sharma, A. Nag and K. V. Adarsh, *J. Phys. Chem. C*, 2017, **121**, 4734–4739.
65 A. Mondal, J. Aneesh, V. K. Ravi, R. Sharma, W. J. Mir, M. C. Beard, A. Nag and K. V. Adarsh, *Phys. Rev. B*, 2018, **98**, 115418.